PMSM Control Based on Finite Set Predictive Current Model Regulation

Li Gang

Sichuan Geely University, Jianyang City, Chengdu 641423
China (Tel: 400-630-2020; e-mail: ligangdzxxgc@guc.edu.cn).

Abstract: Based on the basic principle and design concept of finite set predictive current model control, combined with the principle of model predictive control, a finite set predictive current model regulation control for Permanent Magnet Synchronous motor (PMSM) is established in the current loop part of the vector control system. At the same time, a matrix converter is proposed to replace the traditional inverter model, and a PMSM simulation model based on finite set predictive current model regulation is established. MATLAB/Simulink simulation software is used to verify the superiority of finite set predictive current model regulation control compared with vector control.

Keywords: PMSM; Finite set current prediction; Matrix converter; State estimator; Simulation.

1. INTRODUCTION

With the continuous development of modern industrial technology, Permanent Magnet Synchronous motor (PMSM) is gradually replacing the traditional asynchronous motor and becoming the preferred power drive scheme in many fields (Ravi et al., 2023), such as electric vehicles (Cvetkovski et al., 2022), wind power generation (Larbaoui et al., 2022) and robotics (Chandra et al., 2022). With its high efficiency, high power density and excellent speed regulation performance, PMSM provides strong power support for complex and variable modern control systems. However, in order to give full play to the advantages of PMSM, it is particularly important to conduct in-depth research on PMSM control system to make it more accurate and more stable to adapt to various working conditions (Yudin et al., 2024).

In the vector control system of PMSM, current regulation is a key link (Samokhvalov et al., 2021). The performance, dynamic response and stability of the motor largely depend on the accuracy of the current regulation. In recent years, some international scholars have carried out a large number of studies on current regulation methods.

Sensorless control technology can achieve effective control of the motor by estimating the state and parameters of the PMSM (Heidaripour et al., 2023). This method can not only reduce the complexity of the system, but also improve the dynamic performance and adaptability of the motor. However, this method has some shortcomings, such as difficulty in detecting the initial position of the rotor, sensitivity to parameter changes, limited dynamic performance, high computational complexity and sensitivity to environmental noise.

Adaptive control is a method that can automatically adjust the control parameters according to the changes of system parameters and the influence of external environment (Rodrigo et al., 2023). In the current regulation of PMSM, adaptive control can effectively improve the robustness and adaptability of the system (Aykut and Ayetül, 2023). By designing and implementing various adaptive algorithms, the motor controller can adjust the control strategy in real time according to the actual running state of the motor and the changes of the external environment, so as to realize the precise adjustment of the current. However, there are some shortcomings in this method, such as the complexity of the algorithm, slow convergence speed, robustness challenges, high dependence on parameter initialization, and large demand for computing resources.

With the rapid development of artificial intelligence technology, neural networks and machine learning algorithms have also been widely used in PMSM current regulation (Kenny et al., 2024; Pietrzak and Wolkiewicz, 2023). These methods can achieve accurate control of current regulation by learning and optimizing the dynamic characteristics of the motor. It improves the precision and response speed of current regulation, and provides new ideas and methods for intelligent control of motor. However, there are some shortcomings in this method, such as lack of physical model understanding, large data demand, generalization ability, calculation delay, model instability, and difficulty in optimization and adjustment.

Fault-tolerant control aims to design and implement fault-tolerant strategies so that the motor controller can still maintain a certain performance in the presence of faults (Anbalagan and Joo, 2023). It includes hardware redundancy design, software fault-tolerant algorithm, and fault diagnosis and isolation. Through the application of fault-tolerant control technology, it can ensure that the motor system can still run stably in harsh environment. However, there are some disadvantages in this method, such as increased complexity, decreased motor performance and increased cost.

Model Predictive Control (MPC) is a model-based control method (Dae and Byungki, 2024), which optimizes the control strategy by predicting the future behavior of the motor. In the current regulation of PMSM, MPC method has shown high potential and application value. However, the single model predictive control has the disadvantages of prediction inaccuracy, calculation delay and additional number of parameter adjustments.

In order to solve the above problems, this paper uses the finite set predictive current model regulation technology to realize the control of PMSM. This method uses the system model to predict the future dynamic behavior, and optimizes the calculation according to the prediction results, so as to obtain the optimal control strategy. This method can not only achieve accurate current regulation under multi-variable and multi-constraint conditions, but also effectively improve the dynamic response and robustness of the system. Therefore, the regulation control based on the finite set predictive current model has broad application prospects and important research value.

2. MATHEMATICAL MODEL OF PMSM

Before studying the PMSM control method, it is necessary to establish a suitable PMSM mathematical model (Pranjic and Virtic, 2020). PMSM is a multivariable system with strong nonlinear coupling, and the relationship between variables is complex. It will be very complicated to model according to the actual system, so for the convenience of analysis, the following assumptions should be made when modeling PMSM (Mathematics, 2020):

(1) Assume that there is no damping winding on the motor rotor;

(2) ignoring the influence of temperature change on motor characteristics;

(3) the magnetic saturation of the core and the stator resistance are ignored;

(4) The three-phase stator of PMSM is completely symmetrical and the incoming current is the standard three-phase sinusoidal current.

2.1 Mathematical model of PMSM in two-phase stationary coordinate system

The mathematical model of PMSM in three-phase stationary coordinate system is transformed into the mathematical model of PMSM in two-phase stationary coordinate system by *Clark* transformation (Pígl and Cipín, 2023).

(1) Stator voltage equation:

$$\begin{bmatrix} u_\alpha \\ u_\beta \end{bmatrix} = \begin{bmatrix} R_S & 0 \\ 0 & R_S \end{bmatrix} \psi + \begin{bmatrix} \frac{d\psi_\alpha}{dt} \\ \frac{d\psi_\beta}{dt} \end{bmatrix} \tag{1}$$

(2) Flux equation:

$$\begin{bmatrix} \psi_\alpha \\ \psi_\beta \end{bmatrix} = \begin{bmatrix} L_d \\ L_q \end{bmatrix} \begin{bmatrix} i_\alpha \\ i_\beta \end{bmatrix} + \phi_l \begin{bmatrix} \cos\theta_e \\ \sin\theta_e \end{bmatrix} \tag{2}$$

Where, L_d and L_q are the inductance of d and q axis, and φ_l is the sympathetic flux linkage.

(3) Electromagnetic torque equation:

$$T_e = 1.5P_n\left[\psi_\alpha i_\beta - \psi_\beta i_\alpha\right] \tag{3}$$

2.2 Mathematical model of PMSM in rotating coordinate system

The *Park* transformation (Katzman et al., 2024) is used to transform the PMSM mathematical model in the two-phase stationary coordinate system into the PMSM mathematical model in the rotating coordinate system.

(1) Stator voltage equation:

$$\begin{cases} u_d = R_S i_d + L_d \frac{di_d}{dt} - \omega_e \psi_q \\ u_q = R_S i_q + L_q \frac{di_d}{dt} + \omega_e \psi_d \end{cases} \tag{4}$$

(2) Flux equation:

$$\begin{cases} \psi_d = \omega_e L_d i_d + \omega_e \psi_f \\ \psi_q = L_q i_q \end{cases} \tag{5}$$

(3) Electromagnetic torque equation:

$$T_e = 1.5P_n\left[i_q \psi_f + i_d i_q \left(L_d - L_q\right)\right] \tag{6}$$

3. PMSM VECTOR CONTROL

In this paper, i_d=0 PMSM vector control technology is used (Jayakumar and Bharatiraja, 2022), i_d=0 control is to make the d axis current component equal to 0, only the q axis current component, at this time, the magnetic flux of the permanent magnet synchronous motor is only generated by the permanent magnet. Therefore, the torque can be controlled only by controlling the q axis current component, and the d and q axis current can be decoupled. This control system is relatively simple, and the stator copper loss is large, so it is easy to realize. Therefore, this control method is selected in this paper.

3.1 Matrix converter

In this paper, a matrix converter is designed to replace the traditional inverter, as shown in Fig. 1, the schematic diagram of the basic structure of the matrix converter; As shown in Fig. 2, the schematic diagram of the bidirectional switch tube structure; Among them, IGBT and diode are selected as switching devices for the bidirectional switch tube.

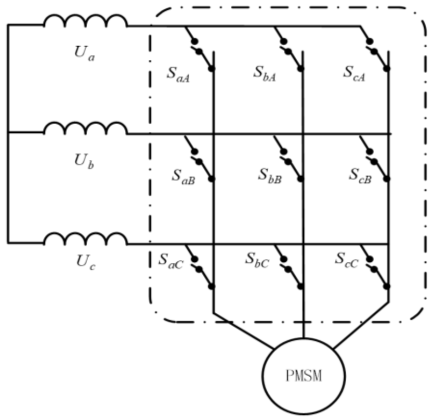

Fig. 1. Schematic diagram of the basic structure of matrix array converter.

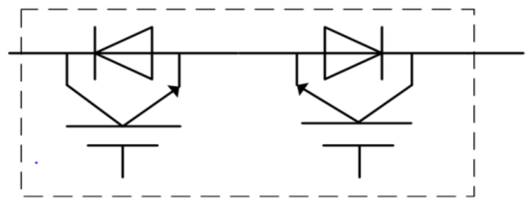

Fig. 2. Schematic diagram of bidirectional switch tube structure.

The specific control algorithm is as follows: using the equivalent method, the matrix converter is regarded as a combination of rectifier and inverter (named as: imaginary converter), as shown in Fig. 3, where rectifier and inverter are not actual device devices. For the convenience of expression and to avoid confusion, the rectifier is called the imaginary rectifier side and the inverter is called the imaginary inverter side.

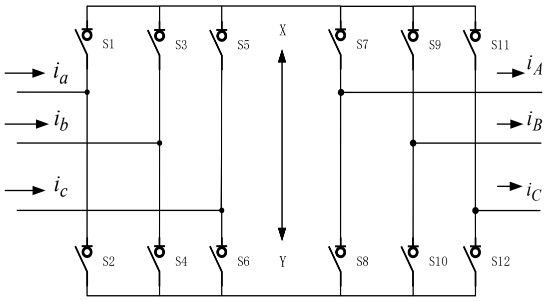

Fig. 3. Switching structure of the imaginary converter.

The open and close states of each bidirectional switch tube of Fig. 1 are defined as follows.

$$S_{mn} = \begin{cases} 1, & open \\ 0, & close \end{cases} \tag{7}$$

Where, $m = \{a, b, c\}$; $n = \{A, B, C\}$.

The equivalent relationship between matrix converter and imaginary converter is as follows.

$$\begin{bmatrix} S_{aA} & S_{bA} & S_{cA} \\ S_{aB} & S_{bB} & S_{cB} \\ S_{aC} & S_{cC} & S_{cC} \end{bmatrix} = \begin{bmatrix} S_7S_1 + S_8S_2 & S_7S_3 + S_8S_4 & S_7S_5 + S_8S_6 \\ S_9S_1 + S_{10}S_2 & S_9S_3 + S_{10}S_4 & S_9S_5 + S_{10}S_6 \\ S_{11}S_1 + S_{12}S_2 & S_{11}S_3 + S_{12}S_4 & S_{11}S_5 + S_{12}S_6 \end{bmatrix} \tag{8}$$

According to (8), the indirect modulation control of the imaginary converter can realize the control of the matrix converter. For the object of study in this paper, only the modulation of the imaginary inverter side needs to be realized.

The a-axis of the three-phase input three-phase current in the time domain coincides with the α-axis in the frequency domain. Taking phase a as the turn-off phase as an example, the current vector is shown in (9):

$$I_s = 1.5(i_a + i_b\alpha + i_c\alpha^2) \tag{9}$$

Where, α is the rotation factor, $\alpha = cos120° + jsin120°$; i_a, i_b, i_c are the three-phase input currents, respectively.

Equation (9) shows that the direction of the current vector is consistent with the direction of the voltage space vector defined by this interval, and by controlling the voltage space vector, the electromagnetic torque can be controlled by controlling the switch tubes S7 to S12.

The non-zero voltage space vector diagram is shown in Fig. 4. When the stator resistance and stator flux are ignored, the expression is:

$$\psi_s(t) = \int \big(V_s(t)\big)dt \tag{10}$$

Where, $V_s(t)$ is the applied voltage space vector in continuous time.

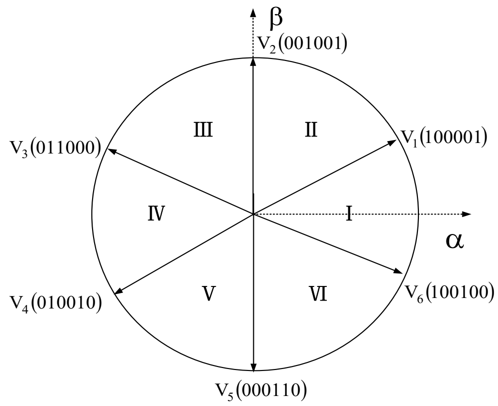

Fig. 4. Non-zero voltage space vector diagram.

Convert (10) into discrete equation form as follows.

$$\psi_s(n+1) = \psi_s(n) + V_s(n)\Delta t \tag{11}$$

Where, n is the sampling time, $\psi_s(n)$ is the stator flux at the current sampling time, $\psi_s(n+1)$ is the stator flux at the next sampling time, $V_s(n)$ is the applied voltage space vector at the current time, Δt is the control period.

3.2 PMSM vector control simulation system

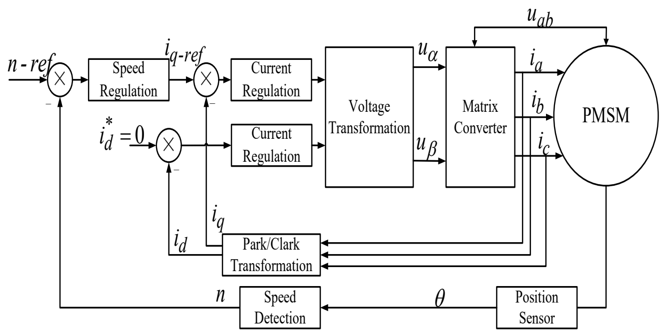

Fig. 5. PMSM Vector control block diagram.

(1) Parameter tuning of speed loop PI controller

The active damping is defined as:

$$i_q = i_q' - B_\alpha\omega_m \tag{12}$$

The vector control strategy adopted in this paper is $i_d=0$, assuming that the motor starts without load, the following can be obtained:

$$\frac{d\omega_m}{dt} = \frac{1.5P_n\psi_f}{J}\left(i_q' - B_\alpha\omega_m\right) - \frac{B}{J}\omega_m \tag{13}$$

Configure the poles of (13) to the desired closed-loop bandwidth β, the transfer function of the rotational speed with respect to the q-axis current can be obtained as follows.

$$\omega_m(S) = \frac{1.5P_n\psi_f}{J(s+\beta)} i_q'(S) \tag{14}$$

By comparing (13) and (14), the coefficient B_α of active damping can be obtained as follows.

$$B_\alpha = \frac{\beta J - B}{1.5 P_n \psi_f} \tag{15}$$

If the traditional PI regulator is used, the expression of the speed loop controller is:

$$i_q^* = \left(\frac{K_{p\omega} - K_{i\omega}}{s}\right)(\omega_m' - \omega_m) - B_\alpha \omega_m \tag{16}$$

Therefore, the parameters $K_{p\omega}$ and $K_{i\omega}$ of PI controller can be set by (17) :

$$\begin{cases} K_{p\omega} = \frac{\beta J}{1.5 P_n \psi_f} \\ K_{i\omega} = \frac{\beta^2 J}{1.5 P_n \psi_f} \end{cases} \tag{17}$$

(2) Parameter tuning of current loop PI controller

The current equation in d and q coordinate system is as follows.

$$\frac{\mathrm{d}i_d}{dt} = \frac{1}{L_d}\left(u_d - B_S i_d + L_q \omega i_q\right) \tag{18}$$

$$\frac{\mathrm{d}i_q}{dt} = \frac{1}{L_q}\left(u_q - R_S i_q - \omega\right)\left(L_d i_d + \phi_f\right) \tag{19}$$

From (18) and (19), it can be concluded that the cross-linked EMF is generated in the q-axis and d-axis directions by the stator current, respectively. If i_d and i_q are completely decoupled, (18) and (19) can be changed into:

$$\begin{cases} u_{d0} = u_d + \omega L_d i_q = R i_q + L_d \frac{di_d}{dt} \\ u_{q0} = u_q - \omega\left(L_d i_d + \psi_f\right) = R i_d + L_q \end{cases} \tag{20}$$

Where, u_{d0} and u_{q0} are the voltages of d and q axis after current decoupling, respectively.

Using a typical PI regulator and a feedforward decoupling control strategy, the voltages in the d and q axes can be achieved as follows:

$$\begin{cases} u_d^* = (K_{pd} + \frac{K_{id}}{s})(i_d^* - i_d) - \omega L_d i_q \\ u_q^* = (K_{pd} + \frac{K_{id}}{s})(i_q^* - i_q) - \omega\left(L_d i_d + \psi_f\right) \end{cases} \tag{21}$$

4. DESIGN OF FINITE SET PREDICTIVE CURRENT MODEL CONTROLLER

4.1 Principle of Model Predictive control

Model predictive control is a control method that based on the mathematical model of the control object (Raphael and Martin, 2023; Panahi et al., 2023; Ritter et al., 2022; Rien and Stefano, 2020), by sampling the current time variable, and relying on the established mathematical model to predict the change of the variable in the future. Considering the influence of the existing controllable variables on the future, through continuous online optimization, the influence caused by model error and uncertain disturbance is overcome, and the stability of the system is improved. It mainly includes three steps: prediction model, rolling optimization and feedback correction, and its structure diagram is shown in Fig. 6.

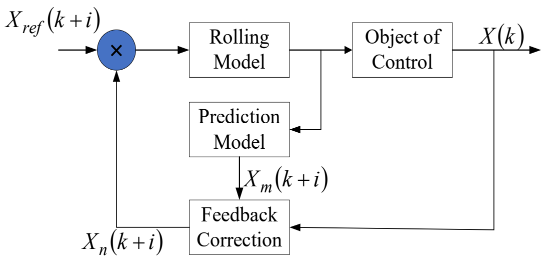

Fig. 6. Model predictive control structure diagram.

4.2 Predictive model

Predictive model control is a control algorithm based on model. The model here is called predictive model, and the predictive model is the foundation and key of the algorithm. In practical applications, prediction models are diversified, which can be differential equations, continuous functions or state equations, and mainly describe the mathematical relationship between input and output. Using the past and future inputs of the controlled plant, the main purpose of the prediction model is to predict the future output. The more the number of prediction steps, the closer the predicted value will be to the actual output. The prediction model can be established as follows.

$$X_n(k+1) = f\left[x(k),\ \ y_n(k)\right] \tag{22}$$

Where, n=1,2,3,4...

4.3 Rolling optimization

Model predictive control solves an optimization problem at each time. The difference between the traditional optimization control and the traditional optimization control is that the traditional optimization control only solves the optimal solution once, while the model predictive control calculates the optimal solution in each sampling period and continuously optimizes in the control time, so it is also called rolling optimization. Therefore, the advantage of the proposed control algorithm is that it can take various uncertain factors into account, effectively improve the stability of the system, and make the controlled object more suitable for the actual needs. The purpose of rolling optimization is to select the optimal control sequence, so we can define a cost function to minimize the error between the predicted value and the reference value, so as to make the best control effect. The cost function is defined as follows:

$$g = |x_{\mathrm{ref}} - x_n(k+1)| + \left|y_{ref} - y_n(k+1)\right| \tag{23}$$

where, n=1,2,3,4...

4.4 Feedback correction

Under the same conditions, the prediction model of model predictive control is only a function prediction model, so there must be an error between the predicted output value of the control algorithm for the future time and the actual expected output value. In order to make the control effect better, feedback correction is very necessary. The essence of the feedback correction is a kind of closed-loop control. The error between the actual output and the expected output in each control period is corrected, so that the output value of the rolling optimization is closer and closer to the expected value.

Feedback correction can be implemented in a variety of ways, including immediately changing the prediction model based on the online recognition principle, or predicting future errors and making corrections while maintaining the prediction model. However, regardless of the correction type, predictive control is based on the optimization of the actual system. An attempt is made to predict and optimize the future dynamic behavior of the system more precisely. Therefore, predictive control is not only based on the system model, but also needs to use the feedback information of the system.

4.5 Finite Set Predictive Current Model Control

In this paper, the current predictive control of permanent magnet synchronous motor is established on the basis of vector control, which is applied to the current loop part of vector control system. The finite set predictive current control block diagram of PMSM is shown in Fig. 7.

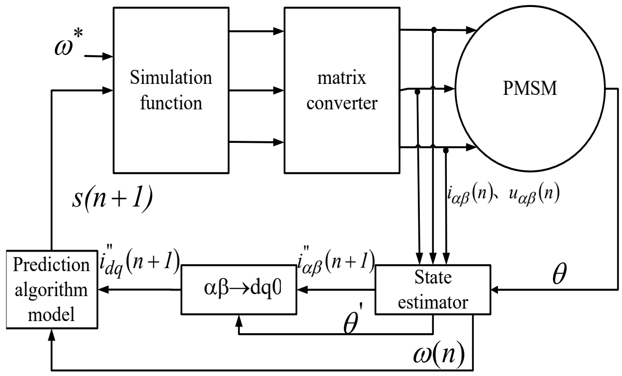

Fig. 7. Control schematic diagram of PMSM finite set predictive current model.

4.6 State estimator algorithm design

The voltage/current sensor, speed/torque sensor and phase detection device can be used to detect the stator current i_α, i_β, as well as the electronic voltage u_α, u_β, and the rotor position θ of the motor, and the sampling period is ts.

And specified: l_s is the stator inductance, ψ_m is the rotor flux, R_s is the stator resistance.

Generally speaking, the rotor position of the motor can only be detected by the speed/torque sensor (Fernandez et al., 2021). At time n, the rotor position is detected as $\theta(n)$ by sampling, and the sampling time is t_s. By using the state estimator, the corresponding relationship between rotor position and speed can be realized.

$$\omega(n) = \frac{\theta(n)-\theta(n-1)}{t_s} \tag{24}$$

The electric signal $u(n)$ detected by the motor at time n and the state estimate $m'(n)$ at time n are used to predict the state vector $m''(n+1)$ at time n+1. The prediction equation is as follows.

$$m''(n+1) = m'(n) + t_s[k(m'(n)) + C(n)u(n)] \tag{25}$$

Where, $m = \begin{bmatrix} i_\alpha \\ i_\beta \\ \omega \\ \theta \end{bmatrix}$, $u = \begin{bmatrix} u_\alpha \\ u_\beta \end{bmatrix}$,

$$k(m) = \begin{bmatrix} -\frac{R_s}{l_s} i_\alpha + \omega \frac{\psi_m}{l_s} \sin\theta \\ -\frac{R_s}{l_s} i_\beta - \omega \frac{\psi_m}{l_s} \cos\theta \\ 0 \\ \theta \end{bmatrix}, \quad C = \begin{bmatrix} \frac{1}{l_s} & 0 \\ 0 & \frac{1}{l_s} \\ 0 & 0 \\ 0 & 0 \end{bmatrix}.$$

Equation (25) is transformed into a state vector only related to the stator current of the motor by matrix transformation:

$$s''(n+1) = \mathrm{D}m''(n+1) \tag{26}$$

Where, $s = \begin{bmatrix} i_\alpha \\ i_\beta \end{bmatrix}$, $D = \begin{bmatrix} 1 & 0 & 0 & 0 \\ 0 & 1 & 0 & 0 \end{bmatrix}$.

The vector prediction value $m''(n+1)$ of the motor is filtered to obtain the optimized correction equation:

$$m'(n+1) = m''(n+1) + Z(n+1)[s(n+1) - s''(n+1)] \tag{27}$$

Where, $s(n+1)$ is the measured value of the motor stator current in the α and β axis components at time n+1; $Z(n+1)$ is the n+1 payoff matrix and $m'(n+1)$ is the motor state vector estimate.

4.7 Model design of current prediction algorithm

Combined with the derived motor state vector estimates, (29) can be derived using (28).

$$m'(n+1) = m(n) + t_s f\big(m(n), u(n)\big) \tag{28}$$

$$m(n+1) = m(n) + t_s/2 \cdot \Big(f\big(m(n), u(n)\big) + f\Big(m'(n+1)\Big), u(n)\Big) \tag{29}$$

Where,

$$f(m,u) = \begin{bmatrix} -1/\tau_s i_d + \omega_r i_q + 1/l_s u_d \\ -1/\tau_s i_q - \omega_r i_d - \psi_m/l_s \omega_r + 1/l_s u_q \\ pK_T/J i_q - N/J \omega_r \end{bmatrix} \tag{30}$$

Where, $\tau_s = l_s / R_s$ is the stator time constant, J is the moment of inertia, N is the damping coefficient, and $K_T = 1.5p\psi_m$ is the motor torque constant.

4.8 Analog function design

$$k = \rho_a(\omega^* - \omega(n+1))^2 + \rho_b\left(i_d^p(n+1)\right)^2 + \rho_c\left(i_{qf}^p(n+1)\right)^2 + k'\left(i_d^p(n+1), i_q^p(n+1)\right) \tag{31}$$

Where, the simulated function $\rho_a(\omega^* - \omega(n+1))^2$ is the following rotor angular velocity target value; $\rho_b(i_d^p(n+1))^2$

is to make the reactive power zero; $\rho_c\left(i_{qf}^p(n+1)\right)^2$ is to try to make the high-frequency part of the torque current zero; $k'\left(i_d^p(n+1), i_q^p(n+1)\right)$ is the amplitude limiting the stator current. The proportional coefficient ρ_a, ρ_b, ρ_c is used to achieve the balance control between different dimensions through the proportional coefficient, so as to adjust the stability of the system.

5. SIMULATION COMPARISON AND ANALYSIS OF THE TWO CONTROL STRATEGIES

5.1 Simulation analysis in steady state

The simulation time is set to 1 s, given a constant speed of 1000 r/min and a constant load torque of 5 N·m, the steady-state simulation results of the motor are shown in Fig. 8. For the convenience of description, the finite set predictive current model control in Figs. 8, 9 and 10 is called "A control" in the following. Vector control is called "B control".

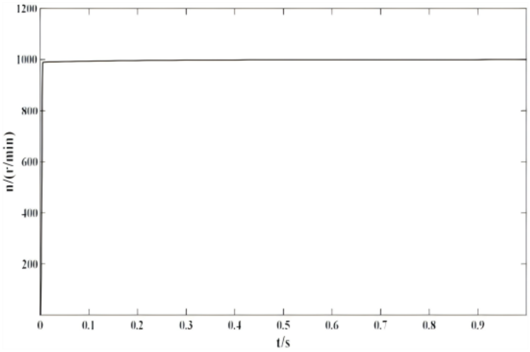

a

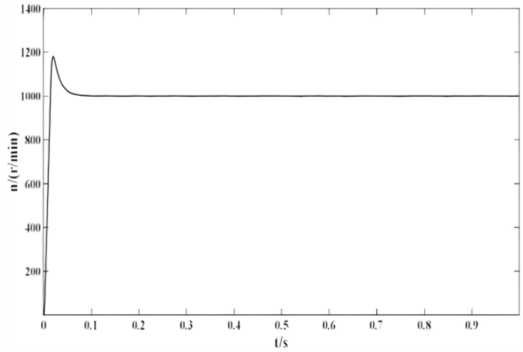

b

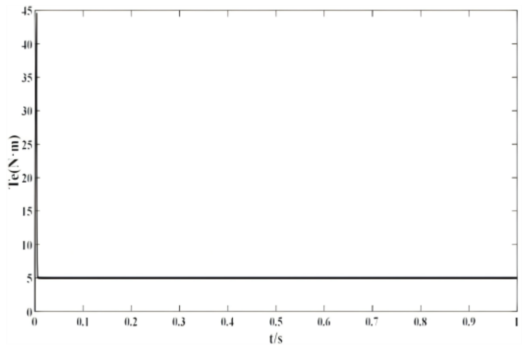

c

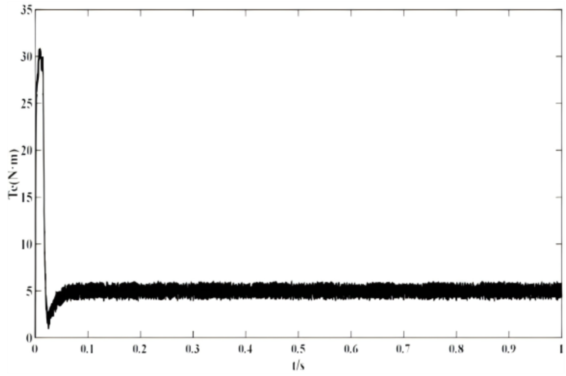

d

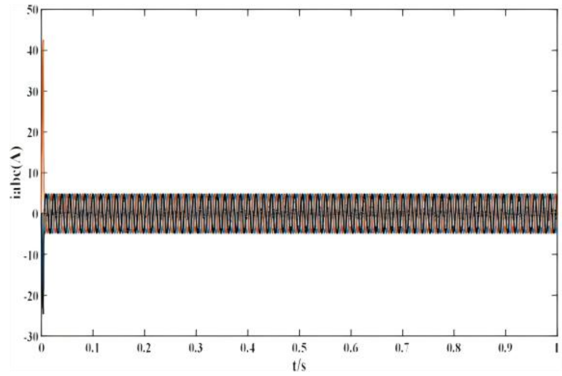

e

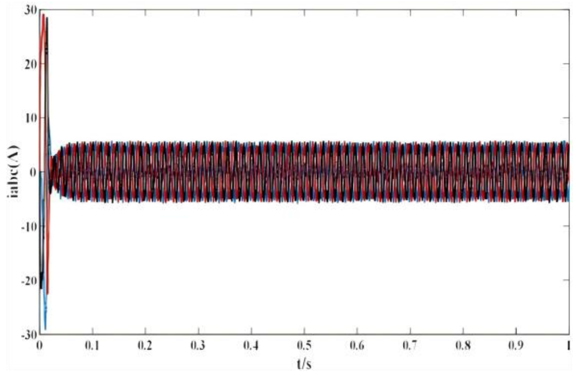

f

Fig. 8. a) motor speed under control of A b) motor speed under control of B c) electromagnetic torque under control of A d) electromagnetic torque under control of B e) three-phase current under control of A f) three-phase current under control of B.

It can be seen from Fig. 8 that when there is no speed change or load change, the finite set predictive current model control can achieve non-overshoot and smooth speed regulation, and the adjustment time is about 0.02 s. The electromagnetic torque can respond quickly, and the three-phase current has no distortion. There is an overshoot of 20% in the speed control of the vector control, and the stability time is about 0.06s. The electromagnetic torque response is slow, the current ripple is large, and the three-phase current has a certain degree of distortion.

5.2 Simulation analysis under variable speed condition

The simulation time is set as 1s, the given speed is 500 r/min, the speed of 0.3 s is changed to 1000 r/min, and the constant load torque is given as 5 Nm. The simulation results of motor speed change are shown in Fig. 9.

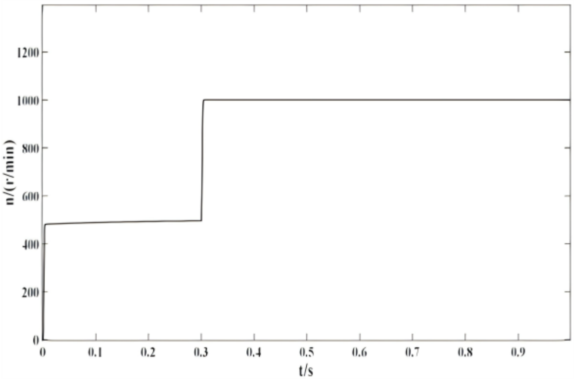

a

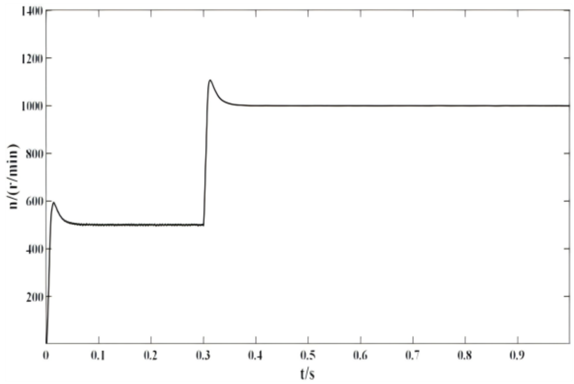

b

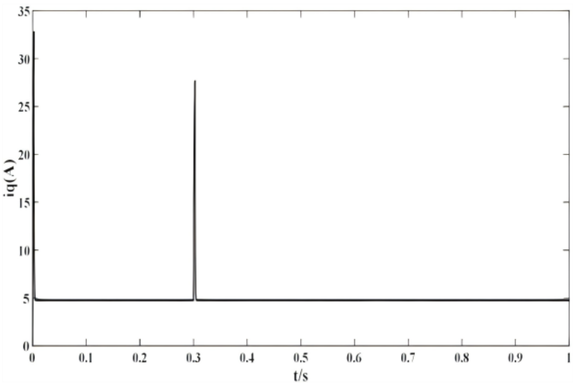

c

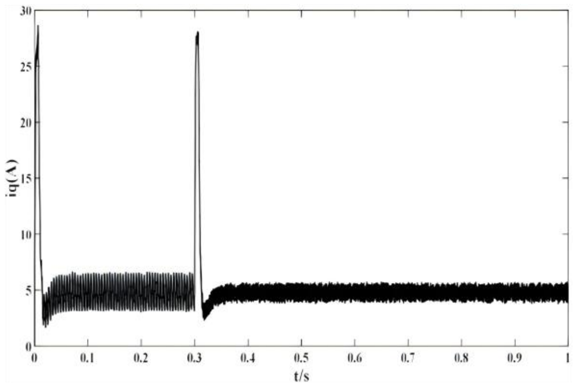

d

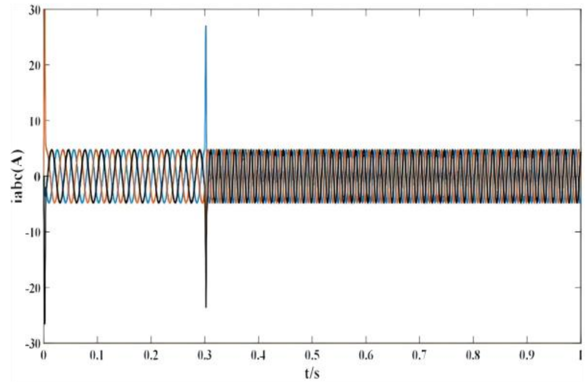

e

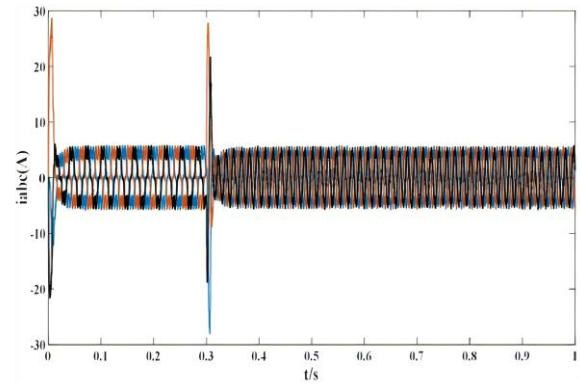

f

Fig. 9. a) motor speed under the control of A b) motor speed under the control of B c) q-axis current under the control of A d) q-axis current under the control of B e) three-phase current under the control of A f) three-phase current under the control of B.

As can be seen from a and b in Fig. 9, under the control of the finite set predictive current model, the motor speed can reach the given speed at about 0.02 s, and it can be seen that there is no overshoot, while under the vector control, the motor speed can reach the given value at about 0.06 s, and there is nearly 20% overshoot. It can be seen from c and d in Fig. 9 that the d-axis currents are basically stable around 0, which is in line with the control strategy of i_d=0. Although the starting peak of q-axis currents under the finite set predictive current model control is larger than that of vector control, it is still within the allowable range of the motor. Under the two control strategies, the electromagnetic torque is proportional to the q-axis current, which is consistent with the electromagnetic torque expression of the motor. However, compared with the finite set predictive current model control, the electromagnetic torque of the vector control is stable, although there is no large overwriting and instability, but the ripple is chaotic.

5.3 Simulation analysis under variable torque condition

The simulation time is 1s, the given constant speed is 1000 r/min, the given load torque is 1 Nm, and the load torque is suddenly increased to 5 Nm in 0.3 s. The simulation results of the motor torque change are shown in Fig. 10.

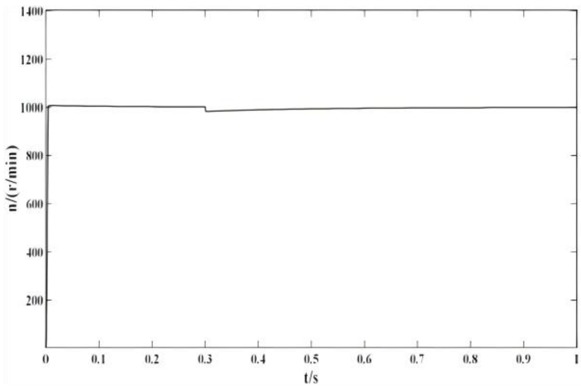

a

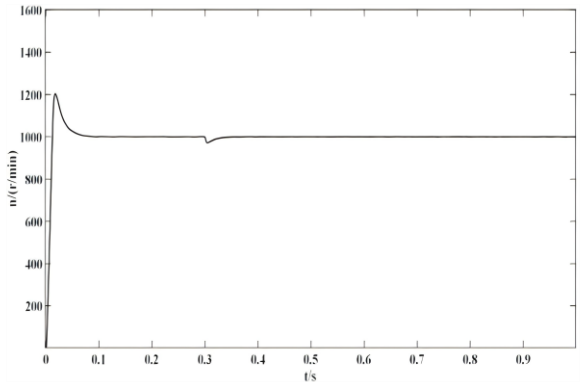

b

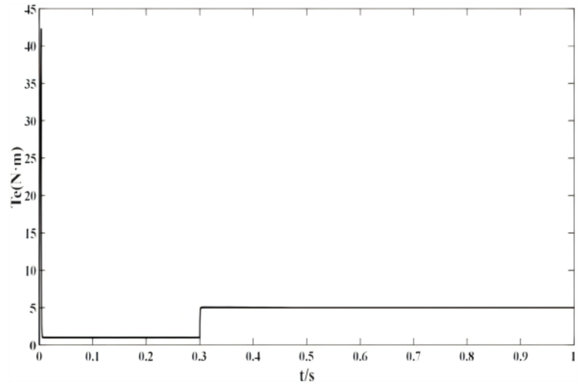

c

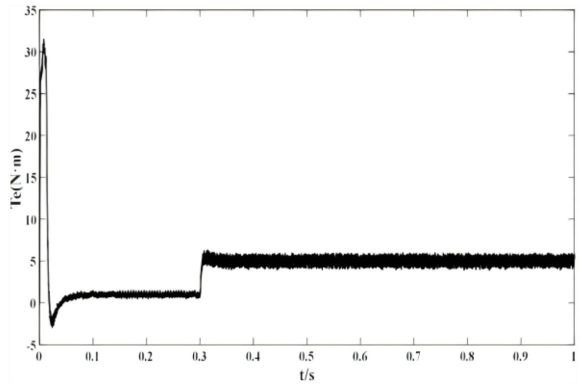

d

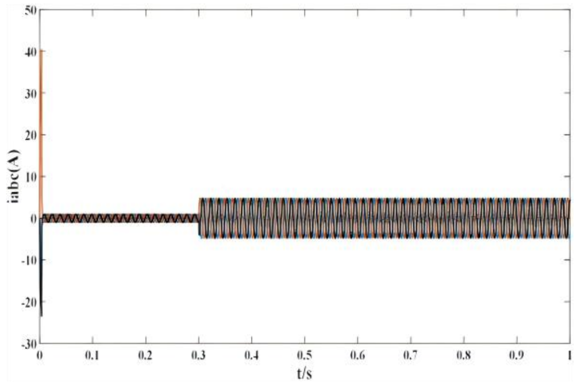

e

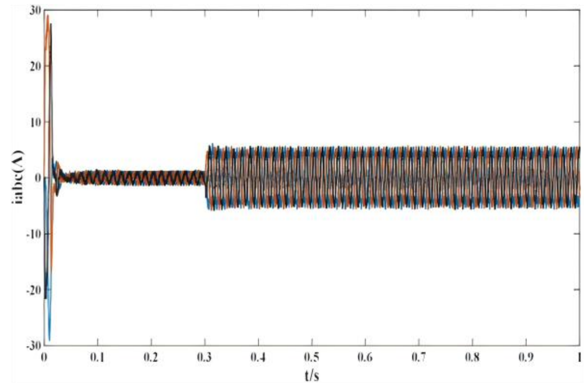

f

Fig. 10. a) motor speed under control of A b) motor speed under control of B c) electromagnetic torque under control of A d) electromagnetic torque under control of B e) three-phase current under control of A f) three-phase current under control of B.

From a and b of Fig. 10, it can be seen that after the sudden change of load torque, the speed is reduced to a certain extent and soon returns to the given speed. However, the motor speed is reduced by about 20rpm under the control of the finite set predictive current model, and the speed of the vector control is reduced by about 40rpm, and the recovery time of the finite set predictive current model control is about 0.03s, and the recovery time of the vector control is about 0.04s. From c and d of Fig. 10, it can be seen that the electromagnetic torque under the control of the finite set predictive current model can achieve a fast and smooth change, while the vector control has an overshoot of about 5% when the torque change returns to stability.

5.4 Simulation analysis under variable speed and variable torque condition

The simulation time was 1 s, the given speed was 1000 r/min, and the loading was carried out to 5 Nm in 0.15 s. 0.3s for loading deceleration to 500 r/min; 0.45s to reduce the load to 2 Nm; The loading speed was accelerated to 800 r/min at 0.6 s. The simulation results are shown in Fig. 11.

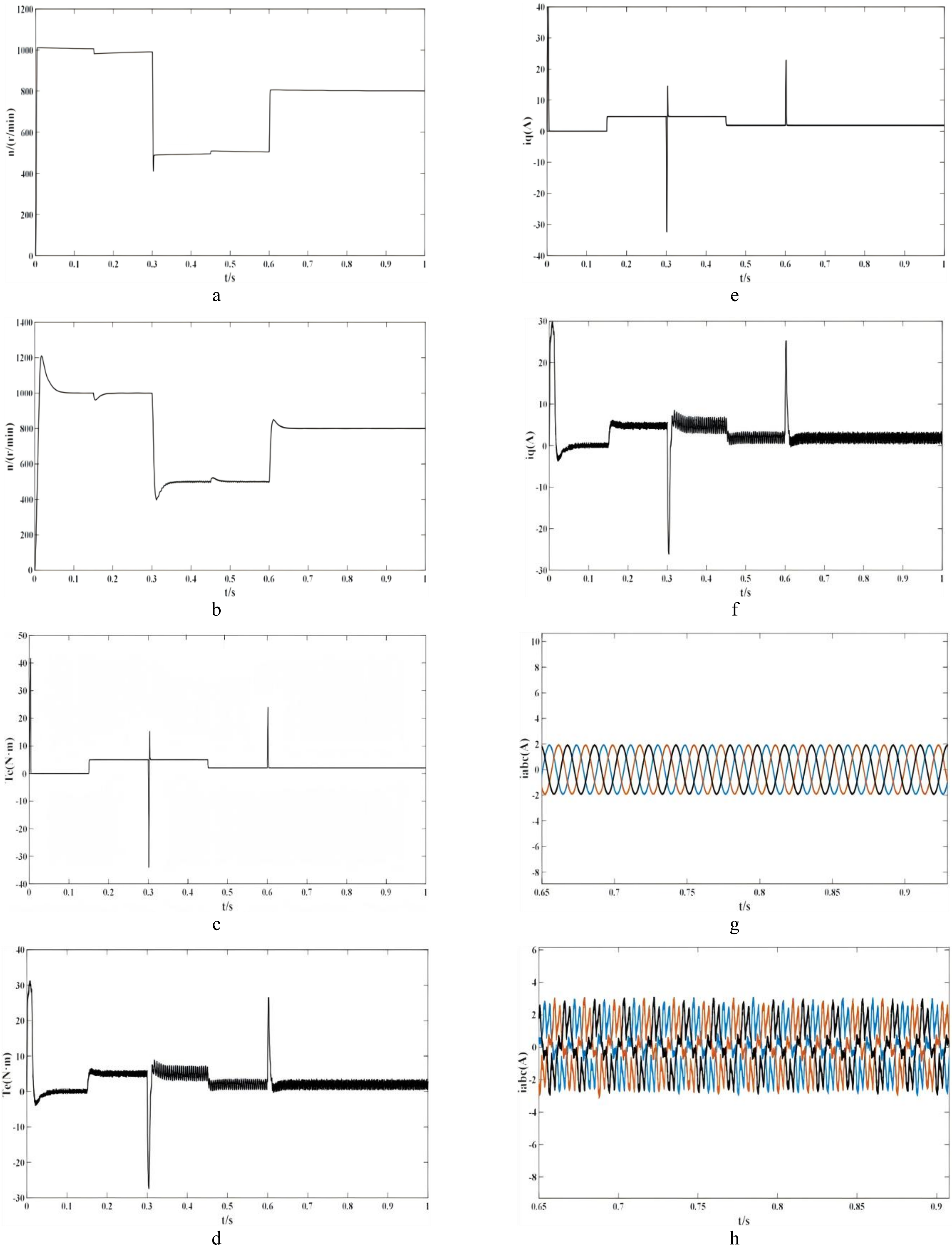

Fig. a) motor speed under the control of A b) motor speed under the control of B c) electromagnetic torque under the control of A d) electromagnetic torque under the control of B e) q-axis current under the control of A f) q-axis current under the control of B g) three-phase current under the control of A h) three-phase current under the control of B.

According to a and b of Fig. 11, when the motor starts, the speed controlled by the finite set predictive current model can reach the given value of 1000 r/min in a very short time, and the overshoot is only 2.1%. However, the traditional vector control takes a long time to reach the given value and the overshoot is 21%. When the subsequent speed and load state change, the finite set model predictive current control can achieve fast and smooth adjustment, while the vector control has large overshoot.

According to c, d, e and f in Fig. 11, the electromagnetic torque is consistent with the previous analysis, and the electromagnetic torque has the same response change with the axis current, and is proportional to the q-axis current. The electromagnetic torque curve of the finite set model predictive current control algorithm changes smoothly, has good dynamic response, and has good dynamic characteristics, while the electromagnetic torque of the vector control algorithm has large fluctuation and low control accuracy in the steady state.

In this paper, the control method with i_d=0 is used, so it can be seen from e and f of Fig. 11 that the current of the d-axis always fluctuates around 0. When the motor starts, the q-axis current stabilization time is 0.01s for the finite set predictive current model control and 0.06 s for the vector control. As a whole, the current of the finite set predictive current model control algorithm changes rapidly with the change of the motor state, and the current pulse fluctuation is less than that of the vector control.

According to g and h in Fig. 11, the three-phase current of vector control has serious distortion and poor current sinicity. The use of finite set predictive current model control algorithm can effectively change the current distortion degree and make it have good sinicity, which reflects that the finite set predictive current model control algorithm has certain optimization effect.

6. CONCLUSIONS

Finite set model predictive current control has unique advantages in dealing with optimization problems under multiple constraints, which can effectively improve the dynamic performance and stability of the motor. This research is not only crucial for improving the performance of motor control, but also has a profound impact on promoting technological progress in related fields. In the fields of electric vehicles, robotics, aerospace and other fields, this technology is expected to reduce energy consumption, improve the overall performance of equipment, and help green and sustainable development. With the continuous development of power electronics technology and continuous innovation of control algorithms, PMSM control based on finite set predictive current model regulation will achieve more efficient and intelligent control. Meanwhile, the introduction of intelligent control technology into motor control is expected to further improve the energy efficiency and reliability of the motor. In general, this research has important practical significance and broad development prospects.

REFERENCES

Anbalagan Pratap and Joo Young Hoon. (2023). Stabilization analysis of fractional-order nonlinear permanent magnet synchronous motor model via interval type-2 fuzzy memory-based fault-tolerant control scheme. *ISA transactions* 310-324.

Aykut Bıçak and Ayetül Gelen. (2023). Modified Super-Twisting Algorithm-Based Model Reference Adaptive Observer for Sensorless Control of the Interior Permanent-Magnet Synchronous Motor in Electric Vehicles. *Machines* (9), 134-156.

Chandra Arabindo, Datta Soumyajit and Chowdhuri Sumana. (2022). Sensorless vector control of PM synchronous motor by hybrid estimation technique considering effect of non-ideal physical attributes. *Electrical Engineering* (5), 3061-3072.

Cvetkovski Goga, Petkovska Lidija, Wiak Sławomir, Di Barba Paolo and Mognaschi Evelina. (2022). Optimal solution of PM synchronous motor obtained by gravitational search algorithm. *International Journal of Applied Electromagnetics and Mechanics* (2), 149-167.

Dae Jin Kim and Byungki Kim. (2024). Linear Matrix Inequality-Based Robust Model Predictive Speed Control for a Permanent Magnetic Synchronous Motor with a Disturbance Observer. *Energies* (4), 223-245.

Fernandez Alonso Daniel, Kang YeGu, Fernandez Laborda Diego, Martinez Gomez Maria, Diaz Reigosa David and Briz Fernando. (2021). Permanent Magnet Synchronous Machine Torque Estimation Using Low Cost Hall-Effect Sensors. *IEEE TRANSACTIONS ON INDUSTRY APPLICATIONS* (4), 3735-3743.

Heidaripour Shahrbjari Behnam, Ghanbari Mahmood, Ebrahimi Reza and Jannati Mohammad. (2023). Sensorless direct vector control technique for induction motor drives under single-phase open-circuit fault. *Electrical Engineering* (4), 2327-2345.

Jayakumar Vinoth and C Bharatiraja. (2022). Model Predictive Control of PMSM Motor Drive for Electric Vehicle Applications with Space Vector Modulation. *Electrochemical Society Transactions* (1), 45-56.

Katzman E. A., Sayan A. S., Bogomolov P. L. and Roumyantzev A. B.. (2024). Influence of Landscape Transformation and the Anxiety Factor on the Distribution of Burrows of the Common Hamster (Cricetus cricetus L., 1758) (Rodentia: Cricetidae) in the Conditions of the Park Zone of the City of Simferopol. *Biology Bulletin* (10), 2630-2638.

Kenny Sau Kang Chu, Kuew Wai Chew, Yoong Choon Chang and Stella Morris. (2024). An Open-Circuit Fault Diagnosis System Based on Neural Networks in the Inverter of Three-Phase Permanent Magnet Synchronous Motor (PMSM). *World Electric Vehicle Journal* (2), 66-78.

Larbaoui Ahmed, Chaouch Djamel Eddine, Belabbes Baghdad and Razkallah Miloud. (2022). Application of passivity-based and sliding mode control of permanent magnet synchronous motor under controlled voltage. *Journal of Vibration and Control* (11-12), 1267-1278.

Mathematics. (2020). Findings from Mohammed V University Broaden Understanding of Mathematics (Robust Multiobjective Model Predictive Control with Computation Delay Compensation for Electric Vehicle Applications Using PMSM with Multilevel Inverter). *Journal of Mathematics*

Panahi Shirin, Kashani Ali and Danielson Claus. (2023). Primal–dual interior-point algorithm for symmetric model predictive control. *Automatica*

Pietrzak Przemyslaw and Wolkiewicz Marcin. (2023). Demagnetization Fault Diagnosis of Permanent Magnet Synchronous Motors Based on Stator Current Signal Processing and Machine Learning Algorithms. *Sensors* (4), 1757-1757.

Pígl Jan and Cipín Radoslav. (2023). Dynamic Model of Medium Voltage Vacuum Circuit Breaker and Induction Motor for Switching Transients Simulation Using Clark Transformation. *Energies* (3), 1020-1020.

Pranjic Franjo and Virtic Peter. (2020). Development of Mathematical Models in Explicit Form for Design and Analysis of Axial Flux Permanent Magnet Synchronous Machines. *APPLIED SCIENCES-BASEL* (21),1345-1348.

Raphael Dyrska and Martin Mönnigmann. (2023). Active set prediction for nonlinear model predictive control on a shrinking horizon based on the principle of optimality. *International Journal of Robust and Nonlinear Control* (4), 2768-2780.

Ravi Eswar Kodumur Meesala, Ramanjaneya Reddy Udumula, Tousif Khan Nizami and Alireza Hosseinpour. (2023). Development of enhanced direct torque control for surface-mounted permanent magnet synchronous motor drive operation. *IET Power Electronics* (11), 1814-1827.

Rien Quirynen and Stefano Di Cairano. (2020). PRESAS: Block-structured preconditioning of iterative solvers within a primal active-set method for fast model predictive control. *Optimal Control Applications and Methods* (6), 2282-2307.

Ritter Andreas, Widmer Fabio, Duhr Pol and Onder Christopher H.. (2022). Long-term stochastic model predictive control for the energy management of hybrid electric vehicles using Pontryagin's minimum principle and scenario-based optimization. *Applied Energy*

Rodrigo Mendoza Becker, Juan Carlos Travieso Torres and Matías Díaz. (2023). Adaptive Control of M3C-Based Variable Speed Drive for Multiple Permanent-Magnet-Synchronous-Motor-Driven Centrifugal Pumps. *Machines* (9), 112-145.

Samokhvalov D. V., Jaber A. I. and Almahturi F. Sh.. (2021). Maximum Power Point Tracking of a Wind-Energy Conversion System by Vector Control of a Permanent Magnet Synchronous Generator. *Russian Electrical Engineering* (3), 163-168.

Yudin R. Y., Petrochenkov A. B., Solodkiy E. M., Vishnyakov D. D. and Salnikov S. V.. (2024). A Study of Finite Control Systems for Permanent-Magnet Synchronous Motors. *Russian Electrical Engineering* (11), 779-785.